Analysis of A Coendemic Model of COVID-19 and Dengue Disease

Hilda Fahlena[1*], Widya Oktaviana[1], Farida[1], Sudirman[1], Nuning Nuraini[1,2], Edy Soewono[1,2]

[1]Faculty of Mathematics and Natural Science, Institut Teknologi Bandung, Bandung, Indonesia
[2]Center for Mathematical Modeling and Simulation, Institut Teknologi Bandung, Bandung, West Java, Indonesia

*Email: hildafahlena@s.itb.ac.id

Abstract

The coronavirus disease 2019 (COVID-19) pandemic continues to spread aggressively worldwide, infecting more than 170 million people with confirmed cases, including more than 3 million deaths. This pandemic is increasingly exacerbating the burden on tropical and subtropical regions of the world due to the pre-existing dengue fever, which has become endemic for a longer period in the same region. Co-circulation dengue and COVID-19 cases have been found and confirmed in several countries. In this paper, a deterministic model for the coendemic of COVID-19 and dengue is proposed. The basic reproduction ratio is obtained, which is related to the four equilibria, disease-free, endemic-COVID-19, endemic-dengue, and coendemic equilibria. Stability analysis is done for the first three equilibria. Furthermore, a condition for coexistence equilibrium is obtained, which gives a condition for bifurcation analysis. Numerical simulations were carried out to obtain a stable limit-cycle resulting from two Hopf bifurcation points with dengue transmission rate and COVID-19 transmission rate as the bifurcation parameter, representing a stable periodic coexistence of dengue and COVID-19 transmission. We identify the period of limit cycle decreases after reaching the maximum value.

Keywords: COVID-19, dengue, SIR model, coendemic, basic reproductive ratio, hopf bifurcation.
2010 MSC classification number: 92D30, 34D23, 37C75

1. INTRODUCTION

Coronaviruses (CoVs) are large enveloped viruses with a single-stranded, unsegmented RNA genome that is positive in sense. It has the largest genome of any RNA. Because CoVs are RNA viruses, they can easily evolve through homologous and non-homologous mutation and recombination, allowing them to spread to a wider range of hosts [1]. COVID-19 was first reported in December 2019 in Wuhan, China, and was declared a pandemic by WHO on March 11, 2020, infecting around 170 million confirmed cases and resulting in over 3 million deaths [2],[3]. Thus, COVID-19 became a disease that emerged with a rapid increase in cases and deaths since the first identification [4]. COVID-19 spreads from person to person via direct contact with sneezing or coughing, or through contact with an infected person's secretions. Therefore, the mechanism of its spread is the same as that of a common cold virus or another influenza [5],[6]. COVID-19 pandemic is a global public health emergency with potentially catastrophic consequences. This pandemic has impacted the burden in tropical and subtropical regions of the world where dengue fever, caused by the dengue virus (DENV), is already prevalent. Concerns have been raised about the similar clinical manifestations of COVID-19 and dengue fever, particularly in dengue-endemic countries [7]. Coexistence of COVID-19 with other illnesses is not uncommon during the COVID-19 pandemic, and misdiagnosis is possible. These problems are particularly prevalent in tropical regions where other infectious illnesses, such as dengue fever, exhibit symptoms comparable to COVID-19[8][9]. In tropical countries, dengue is diagnosed by identifying distinctive symptoms such as fever and test abnormalities such as thrombocytopenia and capillary leakage[10]. Serological assays are being utilized to confirm dengue virus infection at the moment. Nonetheless, the resemblance in some symptoms between dengue and COVID-19, as well as the possibility of cross-reactions in serological testing, might lead to difficulties in diagnosis and is an essential topic to address [11].

Dengue is a common infection in the tropic and subtropic areas that is caused by the dengue virus (DENV) that transmitted by bite mosquitoes of Aedes Aegypty and Aedes albopictus. It is estimated that 400 million

*Corresponding Author
Received November 20^{th}, 2021, Revised December 10^{th}, 2021, Accepted for publication December 24^{th}, 2021.
Published by Indonesian Biomathematical Society, e-ISSN: 2549-2896, DOI:10.5614/cbms.2021.4.2.5

dengue infections occur each year, caused by four antigenically related but distinct viruses, DENV-1, DENV-2, DENV-3, and DENV-4 [12]. Primary infection with one of the serotypes is usually not dangerous, even if some people develop asymptoms [15]. Because there is no immunity, secondary infection by other serotypes can be more severe and lead to life-threatening conditions such as Dengue Haemorrhagic Fever or Dengue Shock Syndrome (DSS) [14]. In recent years, mathematical modeling has become an important tool for understanding the epidemiology and dynamics of infectious diseases. Multi-strain dengue dynamics have been modeled at the population level using extended (susceptible-infected-recovered) SIR-type models that include immunological aspects of the disease such as temporary cross-immunity and ADE phenomenology [15],[16]. Pongsumpun et al. [17] have studied a mathematical model of Dengue Hemorrhagic Fever (DHF) transmission in a two-age structure in the human population, namely Juveniles class and adults class. Nuraini et al. has studied dengue transmission models with two strains involving the role of immunity [18]. In addition, they have also built a within-host model involving cells, viruses, and immunity [19].

Several investigations have found false-positive dengue serology findings in individuals with COVID-19. Coinfection of COVID-19 and dengue have been found and confirmed in several countries, including Argentina with 13 cases, Singapore with 2 cases and Indonesia with 1 case [20],[21],[22]. To simply explain coinfection transmission and when it can occur, mathematical models with various assumptions have been explored and evaluated, with a focus on evaluating the components that allow widespread transmission and controlling for pathogen transmission [24]. We developed the Susceptible-Invected-Recovered model by Kermack and McKendrick in 1927 [25]. One of the tools that facilitate the understanding of the spread of infectious diseases is mathematical modeling. Several mathematical approaches to study the dengue transmission, the COVID transmission and coinfection of COVID-19 and dengue dynamics which Nuraini et al.[26] proposed a mathematical model of dengue internal transmission process, Samui et al.[27] proposed a mathematical model for COVID-19 transmission dynamics with a case study of India, furthermore Masyeni et al.[22] serological cross-reaction and co-infection of COVID-19 and dengue in Asia: experience from Indonesia. Yang et al. [23] developed a mathematical model encompassing two subpopulations based on different fatality rates in young (60 years old or less) and elder (60 years old or more) subpopulations, with the goal of studying the effects of quarantine and further relaxation (release) on the CoVID-19 epidemic. In this study, we propose a SIR-SI mathematical model for coendemic of COVID-19 and dengue in human population that consist of susceptible human, infected dengue human, infected COVID-19 human, recovery dengue human, recovery COVID-19 human, recovery COVID-19 and dengue.

In this model, we will discuss which parameters influence the coendemic occurrence of these two diseases. Furthermore, we derive basic reproductive ratio $(\mathcal{R}_0)$, which represent the endemic ratio of the disease during period. The organization of the rest of this paper is as follows. In Section 2, we construct the mathematical model of a coendemic COVID-19 and dengue. Section 3 presents analysis model. Meanwhile, in Section 4, numerical simulations are proposed to explain the bifurcation, especially the Hopf bifurcation, the existence of the limit cycle, and their period. Finally, Section 5 presents the conclusions

2. MODEL FORMULATION

Herein, we construct a mathematical model for coendemic of COVID-19 and dengue disease in a human population. In this case, the host population is divided into eight subpopulations; susceptible host (S_h), infected dengue (I_d), infected COVID-19 (I_c), infected dengue with COVID-19 immunity (I_{cd}), infected COVID-19 with dengue immunity (I_{dc}), recovery for dengue (R_d), recovery for COVID-19 (R_c), and recovery for dengue and COVID-19 (R_h). The total of host population is denoted by N_h, where $N_h = S_h+I_d+I_c+I_{cd}+I_{dc}+R_d+R_c+R_h$. While the population of vector is divided into two subpopulations are susceptible vector S_v and infected vector I_v, where total population of vector is $N_v = S_v+I_v$. Susceptible host S_h is assumed only infected by either COVID-19 or dengue. Subpopulation R_d and R_c are assumed to get lifelong immunity to dengue but possible to be infected by COVID-19 and get lifelong immunity to COVID-19 but possible to be infected by dengue, respectively. While R is a population with lifelong dengue and COVID-19 immunity.

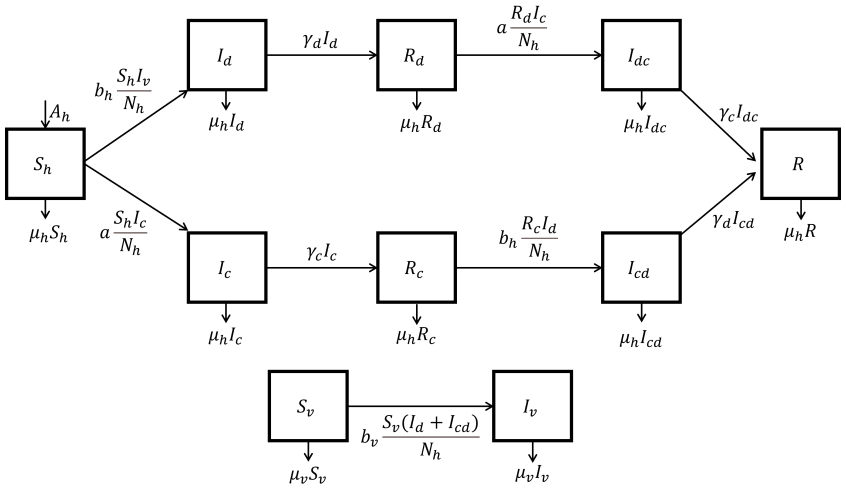

Figure 1: Compartement diagram for coendemic of COVID-19 and dengue.

Based on the above, we construct system of non-linear which describing the dynamic of coendemic COVID-19 and dengue disease, which is given by:

$$
\begin{aligned}
\frac{d\hat{S}_h(t)}{dt} &= A_h - b_h \frac{\hat{S}_h(t)\hat{I}_v(t)}{N_h(t)} - a\frac{\hat{S_h}(t)\hat{I}_c(t)}{\hat{N}_h(t)} - \mu_h \hat{S}_h(t),\\
\frac{d\hat{I}_d(t)}{dt} &= b_h \frac{\hat{S}_h(t)\hat{I}_v(t)}{\hat{N}_h(t)} - \gamma_d \hat{I}_d(t) - \mu_h \hat{I}_d(t),\\
\frac{d\hat{R}_d(t)}{dt} &= \gamma_d \hat{I}_d(t) - a\frac{\hat{R}_d(t)\hat{I}_c(t)}{\hat{N}_h(t)} - \mu_h \hat{R}_d(t),\\
\frac{d\hat{I}_{dc}(t)}{dt} &= a\frac{\hat{R}_d(t)\hat{I}_c(t)}{\hat{N}_h(t)} - \gamma_c \hat{I}_{dc}(t) - \mu_h \hat{I}_{dc}(t),\\
\frac{d\hat{I}_c(t)}{dt} &= a\frac{\hat{S}_h(t)\hat{I}_c(t)}{\hat{N}_h(t)} - \gamma_c \hat{I}_c(t) - \mu_h \hat{I}_c(t),\\
\frac{d\hat{R}_c(t)}{dt} &= \gamma_c \hat{I}_c(t) - b_h \frac{\hat{R_c}(t)\hat{I}_v(t)}{\hat{N}_h(t)} - \mu_h \hat{R}_c(t),\\
\frac{d\hat{I}_{cd}(t)}{dt} &= b_h \frac{\hat{R}_c(t)\hat{I}_v(t)}{\hat{N}_h(t)} - \gamma_d \hat{I}_{cd}(t) - \mu_h \hat{I}_{cd}(t),\\
\frac{d\hat{R}(t)}{dt} &= \gamma_d \hat{I}_{cd}(t) + \gamma_c \hat{I}_{dc}(t) - \mu_h \hat{R}(t),\\
\frac{d\hat{S}_v(t)}{dt} &= A_v - b_v \frac{\hat{S}_v(t)}{\hat{N}_h(t)}(\hat{I}_d(t) + \hat{I}_{cd}(t)) - \mu_v \hat{S}_v(t),\\
\frac{d\hat{I}_v(t)}{dt} &= b_v \frac{\hat{S}_v(t)}{\hat{N}_h(t)}(\hat{I}_d(t) + \hat{I}_{cd}(t)) - \mu_v \hat{I}_v(t),\\
\hat{N}_h(t) &= \hat{S}_h(t) + \hat{I}_d(t) + \hat{R}_d(t) + \hat{I}_{dc}(t) + \hat{I}_c(t) + \hat{R}_c(t) + \hat{I}_{cd}(t) + \hat{R}(t),\\
\hat{N}_v(t) &= \hat{S}_v(t) + \hat{I}_v(t),
\end{aligned}
\tag{1}
$$

where all parameters are positive, $\frac{d\hat{N}_h(t)}{dt} = A_h - \mu_h \hat{N}_h(t)$, and $\frac{d\hat{N}_v(t)}{dt} = A_v - \mu_v \hat{N}_v(t)$. To reduce the

dimension of System (1), we normalize variables by subtituting $S(t) = \frac{\hat{S}(t)}{\hat{N}_h(t)}, I_d(t) = \frac{\hat{I}_d(t)}{\hat{N}_h(t)}, R_d(t) = \frac{\hat{R}_d(t)}{\hat{N}_h(t)}, I_c(t) = \frac{\hat{I}_c(t)}{\hat{N}_h(t)}, R_c(t) = \frac{\hat{R}_c(t)}{\hat{N}_h(t)}$. We assume that the total population $\hat{N}_h(t)$ and $\hat{N}v$ is constant, so we can represent A_h as $\mu_h\hat{N}_h(t)$ and A_v as $\mu_v\hat{N}v$. Further, to reduce the dimension of equation System (1) we normalize which are given as follow:

$$\begin{aligned}
\frac{dS_h(t)}{dt} &= \mu_h - b_h S_h(t) I_v(t) - a S_h(t) I_c(t) - \mu_h S_h(t),\\
\frac{dI_d(t)}{dt} &= b_h S_h(t) I_v(t) - \gamma_d I_d(t) - \mu_h I_d(t),\\
\frac{dR_d(t)}{dt} &= \gamma_d I_d(t) - a R_d(t) I_c(t) - \mu_h R_d(t),\\
\frac{dI_{dc}(t)}{dt} &= a R_d(t) I_c(t) - \gamma_c I_{dc}(t) - \mu_h I_{dc}(t),\\
\frac{dI_c(t)}{dt} &= a S_h(t) I_c(t) - \gamma_c I_c(t) - \mu_h I_c(t),\\
\frac{dR_c(t)}{dt} &= \gamma_c I_c(t) - b_h R_c(t) I_v(t) - \mu_h R_c(t),\\
\frac{dI_{cd}(t)}{dt} &= b_h R_c(t) I_v(t) - \gamma_d I_{cd}(t) - \mu_h I_{cd}(t),\\
\frac{dR_h(t)}{dt} &= \gamma_d I_{cd}(t) + \gamma_c I_{dc}(t) - \mu_h R_h(t),\\
\frac{dS_v(t)}{dt} &= \mu_v - b_v S_v(t)(I_d(t) + I_{cd}(t)) - \mu_v S_v(t),\\
\frac{dI_v(t)}{dt} &= b_v S_v(t)(I_d(t) + I_{cd}(t)) - \mu_v I_v(t),
\end{aligned} \tag{2}$$

where $N_h = 1$ and N_v=1. For the biological meaning, System (2) can be expressed as follow:

$$\frac{dX(t)}{dt} = \mathcal{F}(X(t)), \tag{3}$$

where $X(t) = (S_h(t), I_d(t), R_d(t), I_{dc}(t), I_c(t), R_c(t), I_{cd}(t), R_h(t), S_v(t), I_v(t))^T$ and $\mathcal{F} : \Omega \to \Omega$, with feasible region $\Omega = \{X(t) \in \mathbb{R} \mid 0 \leq x_i \leq 1, i = 1, 2, ..., 10\}$. The most convenient analytical procedure to state the positivity invariant is that investigating the euclidean dot product between outgoing normal vectors to the hyperplane boundaries of the non-negative $2^{10}-$hyperoctant of 10-dimensional Euclidean space and the vector fields of the system along these boundaries. Since the non-positive result of such dot product at all points lying on the coordinate hyperplanes exclude the origin, it will tell us that once the initial condition is taken inside the $2^{10}-$non negative hyperoctant, and if the trajectory touches any boundary afterward, then the trajectory will either return into the interior of this hyperoctant or remain on the boundary for all time and in the future. It follows that the region Ω is positively invariant of System (2). The Parameters used in the model are described in Table 1.

3. ANALYSIS MODEL

In this section, we will discuss model analysis which includes: the basic reproductive ratio, the existence of an equilibrium point and the stability requirements of each equilibrium point.

3.1. Disease-free equilibrium and basic reproductive ratio

The disease-free equilibirum points are steady state solution of the proposed System (2), where there is no disease. We obtain the positive equilibirum human and mosquito population which we will denote by E_0 and it is given by

$$E_0 = (S_h^0, I_d^0, R_d^0, I_{dc}^0, I_c^0, R_d^0, I_{cd}^0, R^0, S_v^0, I_v^0) = (1, 0, 0, 0, 0, 0, 0, 0, 0, 0).$$

Table 1: Description parameters in System (2).

Parameter	Description	Unit	Value	Source
μ_h	Host mortality rate	$\frac{1}{day}$	$\frac{1}{65\times365}$	[28]
μ_v	Vector mortality rate	$\frac{1}{day}$	$\frac{1}{14}$	[29]
a	Transmission rate of COVID-19 infection	$\frac{1}{day}$	[0;1]	Assumed
b_h	Transmission rate of Dengue infection from vector to host	$\frac{1}{day}$	[0;1]	Assumed
b_v	Transmission rate of Dengue infection from host to vector	$\frac{1}{day}$	[0;1]	Assumed
γ_d	Recovery rate of infected dengue	$\frac{1}{day}$	$\frac{1}{10}$	Assumed
γ_c	Recovery rate of infected COVID-19	$\frac{1}{day}$	$\frac{1}{14}$	Assumed

From the disease-free equilibirum, we use next generation matrix (NGM) to define the basic reproductive ratio $\mathcal{R}_0$. The basic reproductive ratio is an average number of secondary infections caused by an infected individual that enter to the fully susceptible population throughout the period of infection. To construct NGM, we only notice the infected compartements $I_{hd}, I_{hdc}, I_{hc}, I_{hcd}, I_v$ and we obtain the following transition Matrix $\mathbf{V}$ and transition Matrix $\mathbf{F}$ follow

$$\mathbf{F} = \begin{bmatrix} 0 & 0 & 0 & 0 & b_h \\ 0 & 0 & 0 & 0 & 0 \\ 0 & 0 & a & 0 & 0 \\ 0 & 0 & 0 & 0 & 0 \\ b_v & 0 & 0 & b_v & 0 \end{bmatrix} \text{ and } \mathbf{V} = \begin{bmatrix} \mu_h+\gamma_d & 0 & 0 & 0 & 0 \\ 0 & \mu_h+\gamma_c & 0 & 0 & 0 \\ 0 & 0 & \mu_h+\gamma_c & 0 & 0 \\ 0 & 0 & 0 & \mu_h+\gamma_d & 0 \\ 0 & 0 & 0 & 0 & \mu_v \end{bmatrix}.$$

We get next generation matrix as follow

$$\mathbf{NGM} = \mathbf{FV^{-1}} = \begin{bmatrix} 0 & 0 & 0 & 0 & \frac{b_h}{\mu_v} \\ 0 & 0 & 0 & 0 & \frac{b_h}{\mu_v} \\ 0 & 0 & 0 & 0 & 0 \\ 0 & 0 & \frac{a}{\gamma_c+\mu_h} & 0 & 0 \\ b_v & 0 & 0 & b_v & 0 \end{bmatrix}.$$

Using the method of Van den Driesche [30] and Diekmann [31], we know that $\mathcal{R}_0$ is calculated by finding the spectral radius of **NGM**

$$\mathcal{R}_0 = max\{\mathcal{R}_{0d}, \mathcal{R}_{0c}\}, \tag{4}$$

where

$$\mathcal{R}_{0d} = \frac{b_v b_h}{\mu_v(\gamma_d+\mu_h)}, \mathcal{R}_{0c} = \frac{a}{\gamma_c+\mu_h}.$$

3.2. Stability analysis of disease-free equilibrium

The disease-free equilibrium point E_0 represents the absence of disease spread in a population, both COVID-19 and Dengue. Stability analysis at point E_0 is given by finding that point on the Jacobian Matrix

as follows

$$\mathbf{J(E_0)} = \begin{bmatrix} -\mu_h & 0 & 0 & 0 & -a & 0 & 0 & 0 & 0 & -b_h \\ 0 & -(\gamma_d+\mu_h) & 0 & 0 & 0 & 0 & 0 & 0 & 0 & b_h \\ 0 & \gamma_d & -\mu_h & 0 & 0 & 0 & 0 & 0 & 0 & 0 \\ 0 & 0 & 0 & -(\gamma_c+\mu_h) & 0 & 0 & 0 & 0 & 0 & 0 \\ 0 & 0 & 0 & 0 & a-(\gamma_c+\mu_h) & 0 & 0 & 0 & 0 & 0 \\ 0 & 0 & 0 & 0 & \gamma_c & -\mu_h & 0 & 0 & 0 & 0 \\ 0 & 0 & 0 & 0 & 0 & 0 & -(\gamma_d+\mu_h) & 0 & 0 & 0 \\ 0 & 0 & 0 & \gamma_c & 0 & 0 & \gamma_d & -\mu_h & 0 & 0 \\ 0 & -b_v & 0 & 0 & 0 & 0 & -b_v & 0 & -\mu_v & 0 \\ 0 & b_v & 0 & 0 & 0 & 0 & b_v & 0 & 0 & -\mu_v \end{bmatrix}$$

and then, we have the characteristic equation of $J(E_0)$ is

$$\begin{aligned} P_0(\lambda) =& (\lambda+\mu_h)^4(\lambda+\mu_v)(\lambda+\gamma_d+\mu_h)(\lambda+\gamma_c+\mu_h)(\lambda+(\mu_h+\gamma_c)(1-\mathcal{R}_{0c})) \\ & (\lambda^2+(\mu_v+\gamma_d+\mu_h)\lambda+\mu_v(\gamma_d+\mu_h)(1-\mathcal{R}_{0d})=0. \end{aligned}$$

The eigenvalue of λ on $P_0(\lambda)$ is negative when $\mathcal{R}_0 < 1$, so the equilibrium point of E_0 is locally asymptotically stable. We deduce that the point E_0 is locally asymptotically stable if $\mathcal{R}_0 < 1$ and a saddle point where $\mathcal{R}_0 > 1$.

3.3. Boundary equilibrium

Boundary equilibrium or endemic equilibirum point of dengue is steady state solution of (2) where the disease of dengue persists in the population. The endemic equilibirum point of dengue is given by

$$E_d = \{S_h^*, I_d^*, R_d^*, 0, 0, 0, 0, 0, S_v^*, I_v^*\} \tag{5}$$

where

$$S_h^* = \frac{\mathcal{R}_{0d}\mu_h + b_h}{\mathcal{R}_{0d}(b_h+\mu_h)}, I_{hd}^* = \frac{\mu_v\mu_h(\mathcal{R}_{0d}-1)}{(b_h+\mu_h)b_v}, R_{hd}^* = \frac{\mu_v(\mathcal{R}_{0d}-1)\gamma_d}{(b_h+\mu_h)b_v},$$

$$S_v^* = \frac{(b_h+\mu_h)}{(\mathcal{R}_{0d}\mu_h+b_h)}, I_v^* = \frac{(\mathcal{R}_{0d}-1)\mu_h}{\mathcal{R}_{0d}\mu_h+b_h}$$

and E_d exist if and only if $\mathcal{R}_{0d} > 1$.

The equilibrium E_c shows the diseases COVID-19 persists in the population with

$$E_c = (S_h^{**}, 0, 0, 0, I_c^{**}, R_c^{**}, 0, 0, 1, 0). \tag{6}$$

where

$$S_h^{**} = \frac{1}{\mathcal{R}_{0c}}, I_c^{**} = \frac{\mu_h}{a}(\mathcal{R}_{0c}-1), R_c^{**} = \frac{\gamma_c}{a}(\mathcal{R}_{0c}-1).$$

We obtain conditions for the existence of positive endemic equilibrium COVID-19 when $\mathcal{R}_{0c} > 1$.

3.4. Stability analysis of dengue boundary equilibrium

Further, we study now the stability of E_d. Endemic equilibrium of dengue E_d is locally asymptotically stable when $\mathcal{R}_{0d} > 1$ and $\mathcal{R}_{0c} < \frac{b_v\mu_h - \mathcal{R}_{0d}(\gamma_d+\mu_h)}{b_v\mu_h-(\gamma_d+\mu_h)} = 1 + \frac{(\gamma_d+\mu_h)(1-\mathcal{R}_{0d})}{b_v\mu_h-(\gamma_d+\mu_h)}$. For more details, see appendix A.

3.5. Stability analysis of COVID-19 boundary equilibrium

Using the linearization method, the characteristic polynomial of the Jacobian Matrix at point E_2 is given as

$$\begin{aligned} P_c(\lambda) =& (\lambda+\mu_h)^2(\lambda+\gamma_c+\mu_h)((\gamma_c+\mu_h)\lambda+\mu_h a)(\lambda+\mu_v)(\lambda+\gamma_d+\mu_h) \\ & (m_0\lambda^2+m_1\lambda+m_2)(n_0\lambda^2+n_1\lambda+n_2)=0, \end{aligned} \tag{7}$$

where
$m_0 = \gamma_c + \mu_h,$
$m_1 = a\mu_h,$
$m_2 = \mu_h(\gamma_c + \mu_h)^2(\mathcal{R}_{0c} - 1),$
$n_0 = a(\gamma_c + \mu_h),$
$n_1 = a\left(\gamma_d + \mu_h + \mu_v\right)\left(\gamma_c + \mu_h\right),$
$n_2 = \left(\gamma_c + \mu_h\right)\mu_v\left(\gamma_d + \mu_h\right)\left(\mathcal{R}_{0c}\gamma_c + \mu_h\mathcal{R}_{0c} - \mathcal{R}_{0c}\gamma_c - \mu_h\mathcal{R}_{0c}\right)$

Based on Equation (7), we deduce that all eigenvalues are negative when $\mathcal{R}_{0c} > 1$ and $\mathcal{R}_{0d} < \frac{\mathcal{R}_{0c}(\gamma_c+\mu_h)}{\mathcal{R}_{0c}\gamma_c+\mu_h} = 1 + \frac{\mu_h(\mathcal{R}_{0c}-1)}{\mathcal{R}_{0c}\gamma_c+\mu_h}$. As a result, this condition reflects stability at the point E_c. The bifurcation diagram in the plane-ab_h is shown in Figure 2 based on the stability conditions for the points E_d and E_c.

3.6. Coendemic equilibrium

In this section, we are interest to find coendemic equilibrium that all subpopulation are not zero. It is shown implicitly by subpopulation I_v as follows

$$E_{co} = (S_h^{***}, I_d^{***}, R_d^{***}, I_{dc}^{***}, I_c^{***}, R_c^{***}, I_{cd}^{***}, R^{***}, S_v^{***}, I_v^{***}) \tag{8}$$

where

$$\begin{aligned}
S_h^{***} &= \frac{\gamma_c + \mu_h}{a} = \frac{1}{\mathcal{R}_{0c}},\\
I_d^{***} &= \frac{b_h\left(\gamma_c + \mu_h\right)I_v^{***}}{a\left(\gamma_d + \mu_h\right)},\\
R_d^{***} &= \frac{I_v^{***}b_h\gamma_d\left(\gamma_c + \mu_h\right)^2}{a\left(\gamma_d + \mu_h\right)\left(\mu_h a - b_h\left(\gamma_c + \mu_h\right)I_v^{***}\right)},\\
I_{dc}^{***} &= \frac{I_v^{***}b_h\gamma_d(\mu_h\left(a - \gamma_c - \mu_h\right) - b_h\left(\gamma_c + \mu_h\right)I_v^{***})}{a(\gamma_d + \mu_h)(\mu_h a - b_h\left(\gamma_c + \mu_h\right)I_v^{***})},\\
I_c^{***} &= \frac{\mu_h(a - \gamma_c - \mu_h)}{a(\gamma_c + \mu_h)} - \frac{b_h(\mu_h + \gamma_c)I_v^{***}}{a(\gamma_c + \mu_h)},\\
R_c^{***} &= \frac{\gamma_c(\mu_h\left(a - \gamma_c - \mu_h\right) - b_h\left(\gamma_c + \mu_h\right)I_v^{***})}{(I_v^{***}b_h + \mu_h)\left(\gamma_c + \mu_h\right)a},\\
I_{cd}^{***} &= \frac{I_v^{***}b_h\gamma_c(\mu_h\left(a - \gamma_c - \mu_h\right) - b_h\left(\gamma_c + \mu_h\right)I_v^{***})}{a(b_h\left(\gamma_d + \mu_h\right)\left(\gamma_c + \mu_h\right)I_v^{***} + \mu_h\left(\gamma_d + \mu_h\right)\left(\gamma_c + \mu_h\right))},\\
R^{***} &= \frac{I_v b_h\gamma_c\gamma_d\left(\gamma_c + a + \mu_h\right)(\mu_h\left(a - \gamma_c - \mu_h\right) - b_h\left(\gamma_c + \mu_h\right)I_v^{***})}{a\left(\gamma_d + \mu_h\right)\left(\gamma_c + \mu_h\right)(I_v^{***}b_h + \mu_h)(\mu_h a - b_h\left(\gamma_c + \mu_h\right)I_v^{***})},\\
S_v^{***} &= \frac{a\mu_v\left(\gamma_d + \mu_h\right)\left(\gamma_c + \mu_h\right)(I_v^{***}b_h + \mu_h)}{b_h b_v\mu_h\left(b_h\left(\gamma_c + \mu_h\right)I_v^{***} + a\gamma_c + \gamma_c\mu_h + {\mu_h}^2\right)}.
\end{aligned}$$

and and the polynomial subpopulation I_v^{***} is

$$P(I_v^{***}) = q_0(I_v^{***})^2 + q_1 I_v^{***} + q_2 = 0, \tag{9}$$

where
$q_0 = {b_h}^2 b_v\mu_h\left(\gamma_c + \mu_h\right)\mu_v,$
$q_1 = b_h\mu_v((\gamma_c + \mu_h)(a\mu_v(\gamma_d + \mu_h) - b_h b_v\mu_h(\gamma_c + \mu_h) + b_v\mu_h^2(\gamma_c + \mu_h) + ab_v\gamma_c\mu_h),$
$q_2 = \mu_v(a{\mu_h}^2\mu_v\left(\gamma_d + \mu_h\right) - b_h b_v{\mu_h}^2\left(\gamma_c + \mu_h\right) - a\gamma_c\mu_h\left(b_h b_v - \mu_v\left(\gamma_d + \mu_h\right)\right)).$
To see that the polynomial $(P(I_v^{***}))$ has one positive root I_v^{***}, observe q_2 with $q_0 > 0$, and then the coefficient q_2 is expressed as follows

$$q_2 = \mu_v^2\mu_h(\gamma_c + \mu_h)(\gamma_d + \mu_h)(\mu_h(\mathcal{R}_{0c} - \mathcal{R}_{0d}) - \mathcal{R}_{0c}\gamma_c(\mathcal{R}_{0d} - 1)). \tag{10}$$

When $\mathcal{R}_{0c} > 1$ and $\mathcal{R}_{0d} > 1 + \frac{\mu_h(\mathcal{R}_{0c}-1)}{\mathcal{R}_{0c}\gamma_c + mu_h}$, the Equation (10) becomes negative. Consider the following form I_c^{***}, which is rewritten as follow

$$I_c^{***} = \frac{\mu_h}{a}(\mathcal{R}_{0c} - 1) - \frac{b_h}{a} I_v^{***}. \tag{11}$$

The form I_c^{***} is positive when $I_v^{***} < \frac{\mu_h}{b_h}(\mathcal{R}_{0c} - 1)$ with $a \neq 0$ and must be $\mathcal{R}_{0c} > 1$ for $I_v^{***} > 0$. This condition also applies to $R_c^{***} > 0$ and $I_{cd}^{***} > 0$. Moreover, the existences of R_d^{***}, I_{dc}^{***}, and R^{***} are obtained when $I_v^{***} < \frac{\mu_h}{b_h}\mathcal{R}_{0c}$. Since $\frac{\mu_h}{b_h}(\mathcal{R}_{0c} - 1) < \frac{\mu_h}{b_h}\mathcal{R}_{0c}$, we can conclude that there is coexistence of equilibrium points when $\mathcal{R}_{0c} > 1, \mathcal{R}_{0d} > 1 + \frac{\mu_h(\mathcal{R}_{0c}-1)}{\mathcal{R}_{0c}\gamma_c + \mu_h}$, and $0 < I_v^{***} < min\{1, \frac{\mu_h}{b_h}(\mathcal{R}_{0c} - 1) = \frac{\mu_h b_v(\mathcal{R}_{0c}-1)}{\mu_v \mathcal{R}_{0d}(\gamma_d + \mu_h)}\}$.

Based on the conditions of existence and stability of the point E_0, E_1, E_2 and the existence of the equilibrium coendemic E_3, a bifurcation diagram in the plane-ab_h is given in Figure 2. For better visualization, we use parameter $b_v = 0.1, \gamma_c = \frac{1}{21}, \gamma_d = \frac{1}{365}, \mu_v = \frac{1}{14}$ in Figure 2(a). However, we also use parameter values according to biological parameters with parameters $b_v = 0.1, \gamma_c = \frac{1}{21}, \gamma_d = \frac{1}{365*70}, \mu_v = \frac{1}{14}$ in Figure 2(b). Figure 2(b) has a very small area III, but Figure 2(b) will be used for bifurcation diagrams in the numerical simulation session later according to its biological parameters.

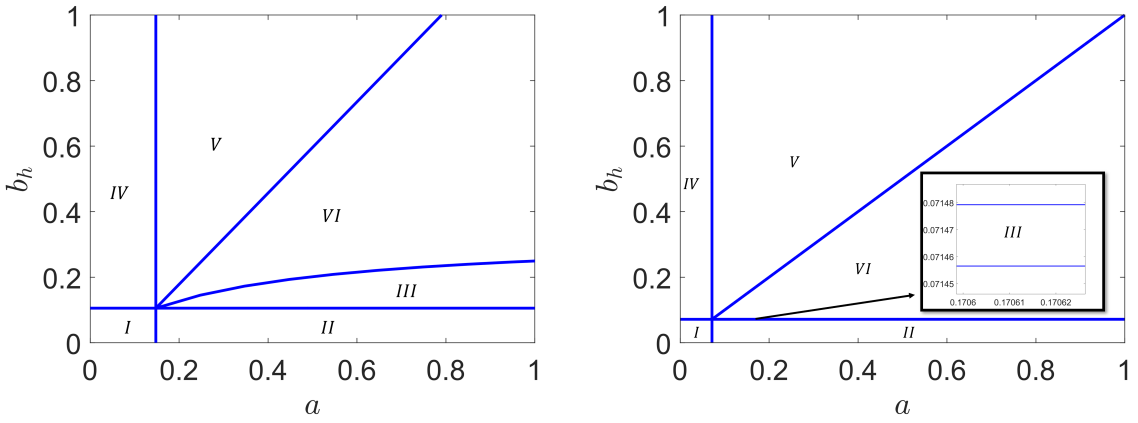

(a) (b)

Figure 2: Diagram of existence of equilibrium E_0, E_d, E_c, E_{co} and their stability with (a) $b_v = 0.05$ (b) $b_v = 0.1$

In Figure 2, there are six region of existence and stability equilibria:

$$\begin{aligned}
I &= \{E_0 \ exist \ and \ stable\},\\
II &= \{E_0 \ exist \ and \ unstable, \ E_c \ exist \ and \ stable\},\\
III &= \{E_0 \ exist \ and \ unstable, \ E_c \ exist \ and \ stable, \ E_d \ exist \ and \ unstable\},\\
IV &= \{E_0 \ exist \ and \ unstable, \ E_d \ exist \ and \ stable\},\\
V &= \{E_0 \ exist \ and \ unstable, \ E_c \ exist \ and \ unstable, \ E_d \ exist \ and \ stable\},\\
VI &= \{E_0 \ exist \ and \ unstable, \ E_c \ exist \ and \ unstable, \ E_d \ exist \ and \ unstable, \ E_{co} \ exist\}.
\end{aligned}$$

4. NUMERICAL SIMULATION

In this session, numerical simulations are given to confirm the analytics that have been discussed in the previous session. In addition, bifurcation diagrams are provided to explain the stability of coendemic points which cannot be found analytically. First, we consider all parameter biology in Table 1 and also parameter $b_v = 0.1$. In Figure 3, we fix parameter $a = 0.4$ and we plot equilibrium I_d and I_c at points E_c (in blue),

E_d (in red) and E_{co} (in magenta) against parameter b_h. This result is consistent with Figure 2(b), when we set $a = 0.4$ and vary the parameter b_h, then there are three regions that are traversed, namely region II (E_c stable), region VI (existence of point E_{co}), and region V (E_d stable). In more detail, Figure 3(a) shows that when $b_h < 0.07145652782$ (condition $\mathcal{R}_d < 1$), point E_c exists and is unstable, and point E_d and E_{co} do not exist. Furthemore, when $b_h^* < b_h < b_h^{*****}$ (see in Figure 3), point E_c is stable and point E_d is not stable. An interesting thing happens when $b_h^{*****} < b_h < b_h^{**}$, there are two points, E_d and E_{co}. In this state, the point E_d is unstable. In contrast to the point E_{co}, it is unstable when $b_h^{***} < b_h < b_h^{****}$, and others are stable under this condition. The stability of this E_{co} point is described in more detail in Figure 4.

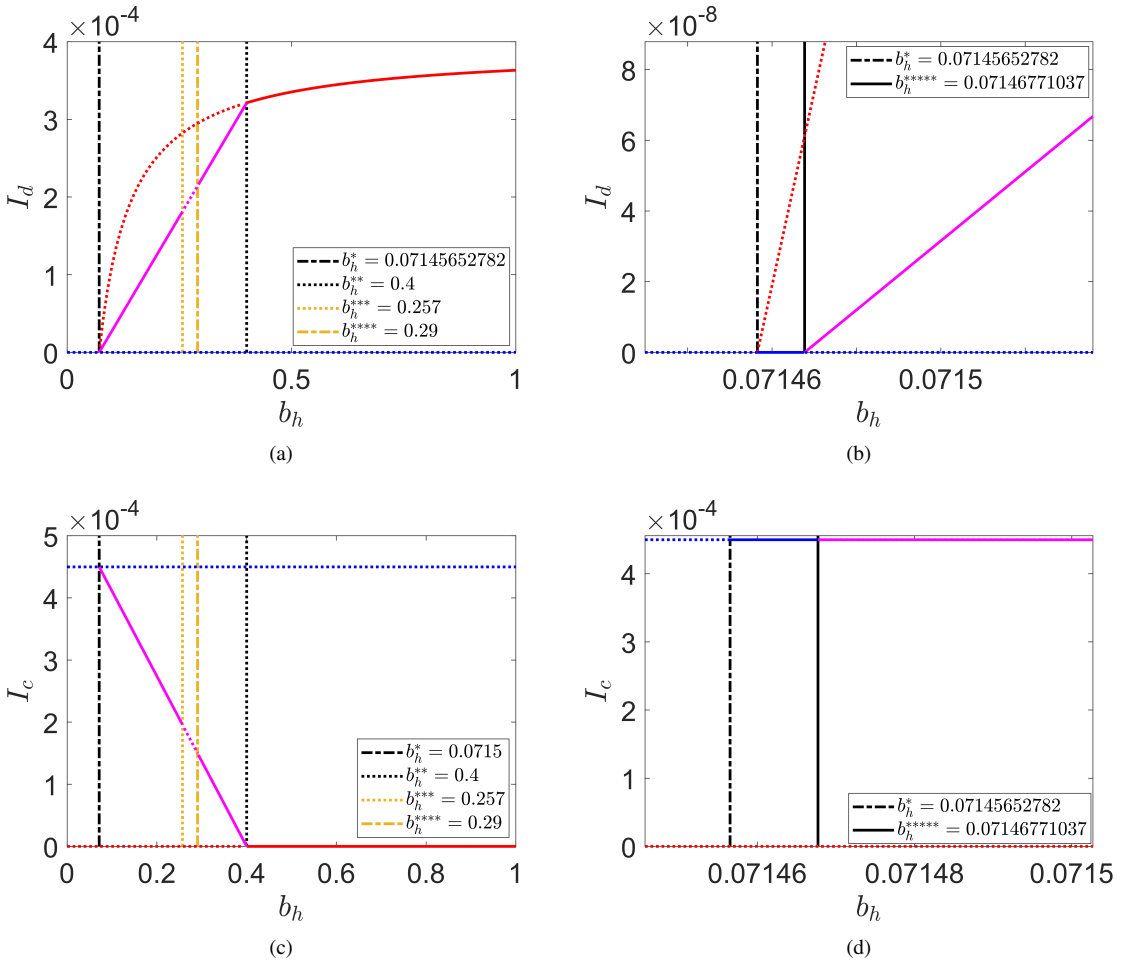

Figure 3: Bifurcation diagram (a) and (c) equilibrium I_d and I_c against parameter b_h, respectively, (b) and (d) equilibrium I_d and I_c against parameter b_h version zoom (a) and (c), respectively, for equilibria E_c (in blue), E_d (in red), and E_{co} (in magenta). Stable equilibrium is marked solid curve and unstable equilibrium is denoted by dashed curve.

We use parameter $b_v = 0.1, \gamma_c = \frac{1}{21}, \gamma_d = \frac{1}{365*70}, \mu_v = \frac{1}{14}, a = 0.4$ in Figure 4. Figure 4 describes the change in the coendemic equilibrium value of I_{cd}^{***} and I_{dc}^{***} against parameter b_h. We use Matcont package in Matlab for simulating bifurcation diagram. In Figure 4, the unstable point has a pair of complex eigenvalues, one of them positive real and non-zero imaginary part, and the others have negative real parts. It is unstable when $0.257 < b_h < 0.29$. There are two Hopf bifurcation points where the real part is zero and

the imaginary part is not zero, when $b_h = 0.257$ and $b_h = 0.29$. We denote these two points as H_1 and H_2, respectively. When $b_h \in (0.257; 0.29)$, they are stable with a pair of complex eigenvalues that real part is negative and the imaginary part is not zero, and the other is negative. Limit cycle exists and is stable when $0.257 < b_h < 0.29$. Figures 4(b) and 4(d) show equilibrium and amplitude when the limit cycle exists. The maximum peak of the limit cycle is $I_{dc}^{***} = 8 * 10^{-4}$ when $b_h = 0.258$ and $I_{cd}^{***} = 13 * 10^{-5}$ at the time of $b_h = 0.26$.

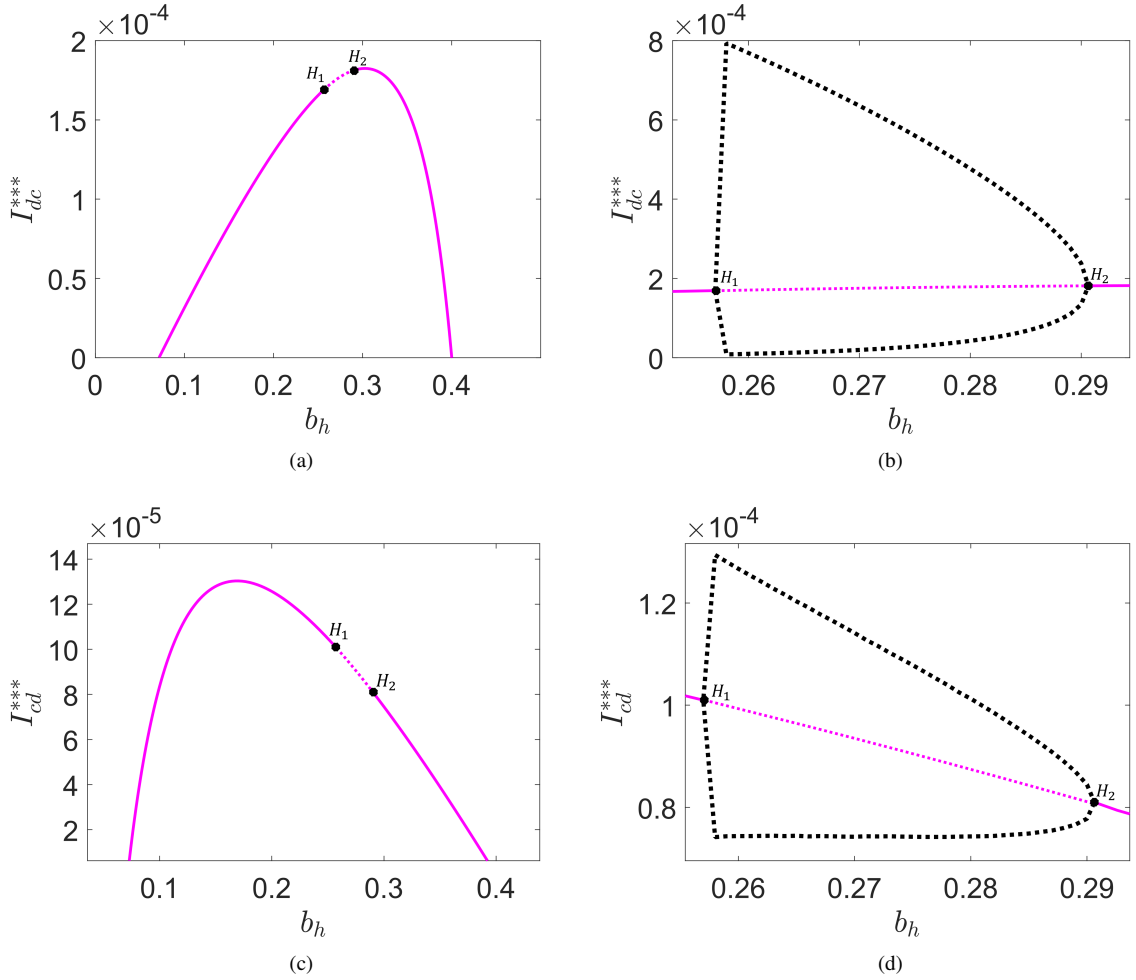

Figure 4: Bifurcation diagram for coexistence equilibrium (a) and (c) I_{dc}^{***} and I_{cd}^{***} against b_h, respectively, (b) and (d) diagram bifurcation zoom version with amplitude. The black dashed curve indicates the maximum and minimum of the periodic solution of System (2). Point H_1 and H_2 label the first Hopf bifurcation and the second Hopf bifurcation.

Figure 4 shows that coendemic conditions exist when the dengue transmission rate from the vector to the host is between 0.05 and 0.38. Coendemic conditions always exist for $t \to \infty$ for the transmission rates of $b_h \in (0.05; 0.257)$ and $b_h \in (0.29; 0.38)$ with a population size infected with dengue after recovering from COVID-19 (population size of infected with COVID-19 after recovering from dengue) is constant. However, at the time of $b_h \in (0.258; 0.29)$, the population sizes of I_{cd} and I_{dc} are not constant but have a period. This condition provides an important warning to us that the maximum number of the infected population must be

considered with the number of hospital facilities stock.

The amplitude in Figure 6 describes the difference between the maximum and minimum I_{cd} and I_{dc} when a limit cycle exists. Increasing the amplitude indicates a large maximum and minimum distance. Figure 6 shows that the amplitude of I_{dc} is greater than the amplitude of I_{cd}. In Figure 5(a), when $b_h = 0.259$, the amplitude of I_{dc} is 0.00078. This means $\frac{78}{10000}$ of the total population and this number is high. This value is quite large for the number of population who experience secondary infection with COVID-19 after recovering from dengue. We also display the period of the limit cycle in Figure 5. The result is that the average period is about 7-9 years. This time is long enough for one period of infection of one population.

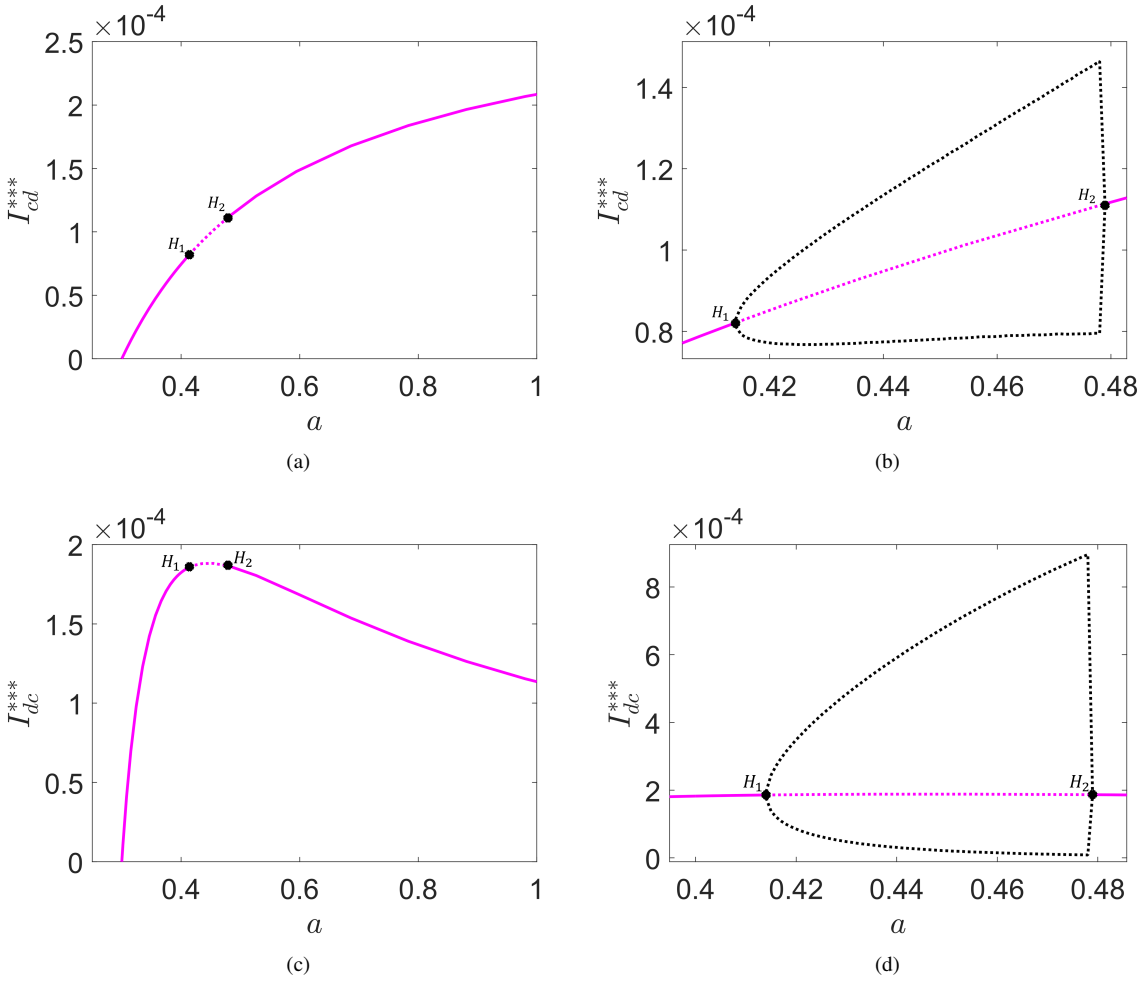

Figure 5: Bifurcation diagram for coendemic equilibrium (a) and (b) I^{***}_{cd} and I^{***}_{dc} against parameter a, respectively, and (b) and (d) diagram bifurcation zoom version with amplitude. The black dashed curve indicates the maximum and minimum of the periodic solution of System (2).

In Figure 5, we set the parameter $b_v = 0.1, \gamma_c = \frac{1}{21}, \gamma_d = \frac{1}{365*70}, \mu_v = \frac{1}{14}, b_h = 0.1$. We also show bifurcation diagram of the coendemic equilibrium point I^{***}_{cd} and I^{***}_{dc} against the parameter a. The existence of a limit cycle between the two Hopf bifurcation points, H_1 and H_2, can also be found by varying parameter a and they are in $a = 0.414$ (H_1) and in $a = 0.479$ (H_2), while others are stable. In contrast to Figure 4, Figure 5 shows that the maximum is greatest when it approaches H_2. In Figure 4 and Figure 5, the

maximum I_{dc}^{***} is higher than the maximum I_{cd}. It means that the number of the population of COVID-19 after recovering from dengue is always higher than the number of population infected with dengue after recovering from COVID-19. Another interesting thing is shown in Figure 6. The period in Figure 6(a) is higher with a variation of parameter b_h than in Figure 6(b) (variation of parameter a). Figure 7 shows the limit cycle (in red), and phase portrait with initial values from inside and outside the limit cycle (in blue).

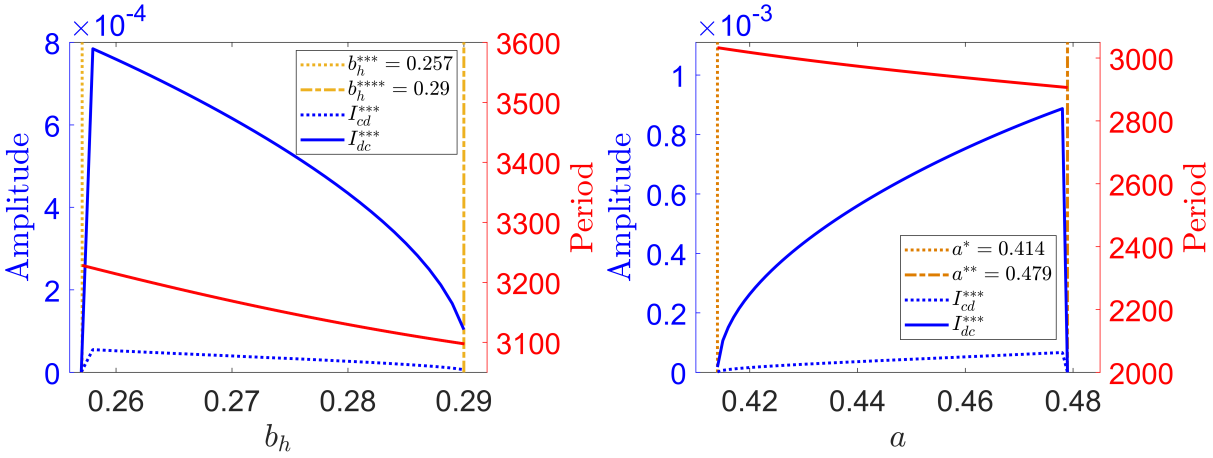

Figure 6: Amplitude and period solution periodic I_{cd}^{***} and I_{dc}^{***} with varied (a) parameter b_h and (b) parameter a.

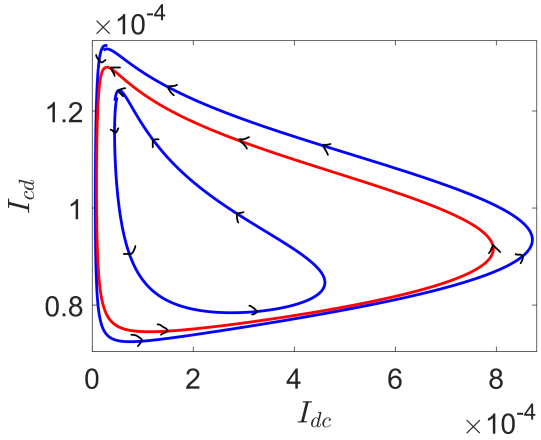

Figure 7: Phase portrait I_{cd} against I_{dc} with parameter $b_v = 0.1, \gamma_c = \frac{1}{21}, \gamma_d = \frac{1}{365*70}, \mu_v = \frac{1}{14}, b_h = 0.258, a = 0.4$.

5. Conclusion

In this paper, we have constructed a coendemic model describing transmission of two pathogens leading to a coendemic phenomenon for dengue and COVID-19 disease. We divided the population into ten compartments: susceptible, infected by dengue, infected by COVID-19, infected by COVID-19 in secondary infection, infected by Dengue in secondary infection recovered from Dengue, recovered from Covid, and recovered from two pathogens. Four equilibria are discussed: pathogen-free equilibrium, two boundary equilibria (single

endemic Dengue, and single endemic COVID-19), and coendemic equilibrium. Basic reproductive ratio $\mathcal{R}_0$ is obtained, followed by the existence of the boundary equilibria when $\mathcal{R}_0 > 1$.

For the coendemic case, we use numerical simulation to determine its stability. Two Hopf bifurcations are found in the coendemic point bifurcation diagram with respect to parameter b_h. The existence of a limit cycle is found between the two Hopf points. The limit cycle periods grow and reach the maximum value and decrease as the coendemicrates increase. Beyond the second Hopf point, the coexistence equilibrium is stable.

ACKNOWLEDGEMENT

HF respectfully acknowledges the financial assistance granted by the Ministry of Research and Technology of Indonesia through the PMDSU Program [grant No. 1511/E4.4/2015]. Part of this work of ES, NN, and HF are funded RistekDikti Doctor Grant 2021 [grant no. 111/IT1.C02/TA.00/2021 and 120L/IT1.C02/TA.00/2021].

APPENDIX A. STABILITY OF E_d

First, we evaluate point E_d in Matrix Jacobian and characteristic equation $P_d(\lambda)$ is given by

$$P_d(\lambda) = (\lambda+\mu_h)^2(\lambda+\mu_v)(\lambda+\gamma_d+\mu_h)(\lambda+\gamma_c+\mu_h)((b_v\mu_h+\gamma_d\mu_v+\mu_h\mu_v)\lambda + b_hb_v\mu_h+b_v{\mu_h}^2)(k_1\lambda+k_2)(l_1\lambda^3+l_2\lambda^2+l_3\lambda+l_4)=0.$$

where

$$\begin{aligned}
k_1 &= -b_v(\mu_h+b_h)\\
k_2 &= a\mu_v(\gamma_d+\mu_h)-b_hb_v(\gamma_c+\mu_h)+b_v\mu_h(a-\gamma_c-\mu_h)\\
&= (\gamma_c+\mu_h)\mu_hb_v(\mathcal{R}_{0c}-1)-(\gamma_c+\mu_h)(\gamma_d+\mu_h)(\mathcal{R}_{0c}-\mathcal{R}_{0d})\\
l_1 &= (\mu_h+b_h)(\gamma_d+\mu_h)(\mu_h(\mu_v+b_v)+\gamma_d\mu_v),\\
l_2 &= (2b_v+\mu_v){\mu_h}^4+((3b_v+\mu_v)b_h+3\gamma_d(\mu_v+b_v))\,{\mu_h}^3\\
&\quad+\left({b_h}^2b_v+\left((4b_v+3\mu_v)\gamma_d+(\mu_v+b_v)^2\right)b_h+{\gamma_d}^2(b_v+3\mu_v)\right){\mu_h}^2\\
&\quad+\gamma_d\left({b_h}^2b_v+((b_v+3\mu_v)\gamma_d+2\mu_v(\mu_v+b_v))b_h+\mu_v{\gamma_d}^2\right)\mu_h+b_h\mu_v{\gamma_d}^2(\mu_v+\gamma_d),\\
l_3 &= \mu_h\mu_v(\gamma_d+\mu_h)(\mathcal{R}_{0d}-1)\left(b_v\gamma_d\mu_h+2b_v{\mu_h}^2+{\gamma_d}^2\mu_v+3\gamma_d\mu_v\mu_h+\mu_v{\mu_h}^2\right)+b_v{\mu_h}^4\mu_v\\
&\quad+b_v\gamma_d{\mu_h}^3\mu_v+{\gamma_d}^2{\mu_h}^2{\mu_v}^2+\gamma_d{\mu_h}^3{\mu_v}^2+b_v\mu_h({b_h}^2b_v\mu_h+{b_h}^2{\gamma_d}^2+2{b_h}^2\gamma_d\mu_h+{b_h}^2\gamma_d\mu_v\\
&\quad+{b_h}^2{\mu_h}^2+{b_h}^2\mu_h\mu_v+2b_h\gamma_d{}^2\mu_h+4b_h\gamma_d{\mu_h}^2+2b_h{\mu_h}^3+b_h\mu_h{}^2\mu_v+{\gamma_d}^2{\mu_h}^2+2\gamma_d{\mu_h}^3+{\mu_h}^4),\\
l_4 &= \mu_h(\gamma_d+\mu_h)^2(\mu_h(\mu_v+b_v)+\gamma_d\mu_v)(\mu_h+b_h)\mu_v(\mathcal{R}_{0d}-1).
\end{aligned}$$

Observe that $l_1, l_2, l_3, l_4 > 0$ when $\mathcal{R}_{0d} > 1$. Further, it can be seen that

$$l_2l_3 > (\gamma_d+\mu_h)^3(b_v\mu_h+\gamma_d\mu_v+\mu_h\mu_v)^2(\mu_h+b_h)^2\mu_h\mu_v(\mathcal{R}_{0d}-1) = l_1l_4.$$

Using Routh-Hurtwitz criteria, the roots of characteristic polynomial of $P_d(\lambda)$ have negative real part when $\mathcal{R}_{0d} > 1$ and $\mathcal{R}_{0c} < \frac{b_v\mu_h-\mathcal{R}_{0d}(\gamma_d+\mu_h)}{b_v\mu_h-(\gamma_d+\mu_h)} = 1+\frac{(\gamma_d+\mu_h)(1-\mathcal{R}_{0d})}{b_v\mu_h-(\gamma_d+\mu_h)}$. Therefore the endemic equilibrium E_d is locally asymptotically stable.

REFERENCES

[1] Felsenstein, S., Herbert, J. A., McNamara, P. S., and Hedrich, C. M., COVID-19: Immunology and treatment options, Clinical immunology, 215, p. 108448, 2020.

[2] Lopes, A. G., Celestino, C. S., Barros, T. T., Fevereiro, A. G., Gejer, D. H., Oliveira, F. M., ... and Amano, M. T., Case Report: A Severe SARS-CoV-2 Infection in a Teenager With Angelman Syndrome, Frontiers in Medicine, 8, p. 108, 2021

[3] "WHO Coronavirus (COVID-19) Dashboard, WHO Coronavirus (COVID-19) Dashboard With Vaccination Data", https://covid19.who.int/, Accessed on June 09, 2021.

[4] Rasmussen, Sonja. A et al., Coronavirus Disease 2019 (COVID-19) and pregnancy: what obstetricians need to know, American Journal of Obstetrics and Gynecology, 2020. https://doi.org/10.1016/j.ajog.2020.02.017, Accessed on June 12, 2021).

[5] Scientific, W. H. O., Heymann, D. L., and Shindo, N., COVID-19: what is next for public health?. Lancet, 395(10224), pp. 542-545, 2020.

[6] Ali, M. Y., Gatiti, P., The COVID-19 (Coronavirus) pandemic: reflections on the roles of librarians and information professionals, Health information and libraries journal, 37(2), pp.158-162, 2020.

[7] Harapan, H., Ryan, M., Yohan, B., Abidin, R. S., Nainu, F., Rakib, A., ... and Sasmono, R. T., Covid-19 and dengue: Double punches for dengue-endemic countries in Asia, Reviews in medical virology, 31(2), p.e2161, 2021.

[8] Chen, N., Zhou, M., Dong, X., Qu, J., Gong, F., Han, Y., ... & Zhang, L., Epidemiological and clinical characteristics of 99 cases of 2019 novel coronavirus pneumonia in Wuhan, China: a descriptive study, The lancet, 395(10223), pp. 507-513, 2020.

[9] Joob, B., Wiwanitkit, V., COVID-19 can present with a rash and be mistaken for dengue, Journal of the American Academy of Dermatology, 82(5), p. e177, 2020.

[10] World Health Organization, et al. Dengue: guidelines for diagnosis, treatment, prevention and control, World Health Organization, 2009.

[11] Yan, G., Lee, C. K., Lam, L. T., Yan, B., Chua, Y. X., Lim, A. Y., and Tambyah, P. A., Covert COVID-19 and false-positive dengue serology in Singapore, The Lancet Infectious Diseases, 20(5), p. 536, 2020.

[12] Bhatt, S., Gething, P. W., Brady, O. J., Messina, J. P., Farlow, A. W., Moyes, C. L., and Hay, S. I., The global distribution and burden of dengue, Nature, 496(7446), pp. 504-507, 2013.

[13] Halstead, S. B., Dengue hemorrhagic fever: two infections and antibody dependent enhancement, a brief history and personal memoir, Revista cubana de medicina tropical, 54(3), pp. 171-179, 2002.

[14] Rothman, A. L., Dengue: defining protective versus pathologic immunity, The Journal of clinical investigation, 113(7), pp. 946-951, 2004.

[15] Halstead, S. B., Katzelnick, L. C., Russell, P. K., Markoff, L., Aguiar, M., Dans, L. R., Dans, A. L., Ethics of a partially effective dengue vaccine: Lessons from the Philippines. Vaccine, 38(35), pp. 5572-5576, 2020.

[16] Aguiar, M., Ballesteros, S., Kooi, B. W., and Stollenwerk, N. The role of seasonality and import in a minimalistic multi-strain dengue model capturing differences between primary and secondary infections: complex dynamics and its implications for data analysis, Journal of theoretical biology, 289, pp. 181-196, 2011.

[17] Pongsumpun, P., and Tang, I. M., Transmission of dengue hemorrhagic fever in an age structured population, Mathematical and Computer Modelling, 37(9-10), pp. 949-961, 2003.

[18] Nuraini, N., Soewono, E., and Sidarto, K. A., Mathematical model of dengue disease transmission with severe DHF compartment, Bulletin of the Malaysian Mathematical Sciences Society, 30(2), 2007.

[19] Nuraini, N., Tasman, H., Soewono, E., and Sidarto, K. A., A with-in host dengue infection model with immune response, Mathematical and Computer Modelling, 49(5-6), pp. 1148-1155, 2009.

[20] Carosella, L. M., Pryluka, D., Maranzana, A., Barcan, L., Cuini, R., Freuler, C., Stryjewski, M. E., Characteristics of Patients Co-infected with Severe Acute Respiratory Syndrome Coronavirus 2 and Dengue Virus, Buenos Aires, Argentina, March–June 2020, Emerging Infectious Diseases, 27(2), p. 348, 2021.

[21] Coronavirus disease 2019 (COVID-19) Situation Report - 69. World Health Organization. https://www.who.int/emergencies/diseases/novelcoronavirus-2019/situation-reports/, published March 29, 2020, Accessed March 30, 2020.

[22] Masyeni, S., Santoso, M. S., Widyaningsih, P. D., Asmara, D. W., Nainu, F., Harapan, H., and Sasmono, R. T, Serological cross-reaction and coinfection of dengue and COVID-19 in Asia: Experience from Indonesia, International Journal of Infectious Diseases, 102, pp. 152-154, 2021.

[23] Yang, H. M., Junior, L. L., Castro, F. F. M., and Yang, A. C., Mathematical model describing CoViD-19 in São Paulo, Brazil–evaluating isolation as control mechanism and forecasting epidemiological scenarios of release, Epidemiology and Infection, 148, 2020.

[24] Anderson, R. M., and May, R. M., Infectious diseases of humans: dynamics and control, Oxford university press, 1992.

[25] Kermack, W. O., McKendrick, A. G., A contribution to the mathematical theory of epidemics, Proceedings of the royal society of London, Series A, Containing papers of a mathematical and physical character, 115(772), pp. 700-721, 1927.

[26] Nuraini, N., Soewono, E., and Sidarto, K. A., A mathematical model of dengue internal transmission process, Journal of the Indonesian Mathematical Society, 13(1), pp. 123-132, 2007.

[27] Samui, P., Mondal, J., and Khajanchi, S., A mathematical model for COVID-19 transmission dynamics with a case study of India, Chaos, Solitons and Fractals, 140, p. 110173, 2020.

[28] Fauzi, I. S., Fakhruddin, M., Nuraini, N., and Wijaya, K. P., Comparison of dengue transmission in lowland and highland area: Case study in Semarang and Malang, Indonesia, Communication in Biomathematical Science, 2(1), pp. 23-37, 2019.

[29] Chávez, J. P., Götz, T., Siegmund, S., and Wijaya, K. P., An SIR-Dengue transmission model with seasonal effects and impulsive control, Mathematical biosciences, 289, pp. 29-39, 2017.

[30] Van den Driessche, P., and Watmough, J., Reproduction numbers and sub-threshold endemic equilibria for compartmental models of disease transmission, Mathematical biosciences, 180(1-2), pp. 29-48, 2002.

[31] Diekmann, O., Heesterbeek, J. A. P., and Metz, J. A., On the definition and the computation of the basic reproduction ratio R 0 in models for infectious diseases in heterogeneous populations, Journal of mathematical biology, 28(4), pp. 365-382, 1990.